2005

Electrochemical Detection of Nanoscale Phase Separation in Binary Self-Assembled Monolayers

R. Carlisle Chambers
George Fox University, cchamber@georgefox.edu

Christina E. Inman
University of Oregon

James E. Hutchison
University of Oregon

Recommended Citation
Previously published in Langmuir, 2005, vol. 21, pp. 4615-4621 http://pubs.acs.org/doi/pdf/10.1021/la050104t

Electrochemical detection of nanoscale phase separation in binary self-assembled monolayers

R. Carlisle Chambers, [a*] *Christina E. Inman,* [b] *and James E. Hutchison* [b*]

a Department of Chemistry, George Fox University, Newberg, Oregon 97132

b Department of Chemistry and Materials Science Institute, University of Oregon, Eugene, Oregon 97403

RECEIVED DATE

Abstract

Developing methods to probe the nature and structure of nanoscale environments continues to be a challenge in nanoscience. We report a cyclic voltammetry investigation of internal, hydrogen-bond driven phase separation of amide-containing thiols and alkane thiols. Amide-containing thiols with a terminal ferrocene carboxylate functional group were investigated in two binary monolayers, one homogeneously mixed and the other phase separated. The electrochemical response of the ferrocene probe was used to monitor adsorbate coverage, environment and phase separation within each of these monolayers. The results demonstrate that the behavior of ferrocene containing monolayers can be used to probe nanoscale organization.

Introduction

The development of materials with high-density, two-dimensional nanoscale features is the current focus of research with applications including nanoelectronics, sensors, and surface biocompatability.[1-13] As part of this research, self-assembled monolayers (SAMs) of alkanethiols on gold surfaces have been widely investigated because they offer well-defined systems that can be used to manipulate interfacial properties and structures on the molecular level.[1-13] Numerous techniques have been used to prepare well-defined, two-dimensional, nanometer-scale structures in thiol/Au SAMs: "soft" lithography techniques such a micro-contact printing,[2,3] selective electrochemical reductive desorption of binary SAMs[4-6] followed by back-filling with an electroactive adsorbate,[5,6] DIP-PEN[6,7] and other scanning probe lithography techniques,[8-10] and chemically-driven phase separation of mixed thiol systems into discrete domains.[12,14,15] Recently, we reported phase separation driven by buried, intermolecular hydrogen-bond interactions between thiols that contain amide groups.[11,12] The buried amide group leaves the ω-functional group available for further elaboration.

Before phase separated monolayers can be incorporated into new materials applications, reliable methods must be developed that are able to probe organization and chemical environment on the nanoscale. A number of analytical techniques have traditionally been used to detect and quantify phase separated domains in both biological and non-living systems, including microscopy,[3,12,15-19] fluorescence,[17-20] spin labels,[21,22] and electrochemistry.[4,5,23-27] While scanning probe techniques (STM, AFM, LFM) can be used to determine domain size on the nanometer scale and smaller, [3,12,15-19] these techniques typically require significant time investment such that evaluation of the entire

sample is rarely feasible. STM also requires that substrate be made of a conducting material and that the molecule(s) used to modify the substrate are short enough to allow for sufficient tunneling to occur between the tip and the substrate.[11,12] Fluorescence techniques have been used to characterize domain size in phase-separated lipid systems[15,20] and to study photoinduced electron and energy transfer mechanisms in thiol/Au SAMs.[27-30] Fluorescence microscopy, however, is limited to structures ≥500 nm in diameter,[18] and quenching by the gold substrate complicates analysis of these systems.[28,29] The strong distance dependence of spin-spin interactions has also allowed electron paramagnetic resonance to be used to characterize nanscale interactions within nanoparticle ligand shells[21] and membranes[22] containing spin labeled molecules. Unfortunately, the low surface area of planar monolayer samples does not allow this method of characterization.

Kakiuchi et al. developed an electrochemical method for probing phase separation based on the potential dependence of the reductive desorption of thiols.[5] They were able to use this technique to assess phase separation in binary, alkanethiol monolayers with different terminal functionalities, create artificially phase separated monolayers, and investigate adsorbate interdiffussion within these assemblies. However, this characterization method is destructive and limited to studying phase separated monolayers where each component has a significantly different reduction potential and the phase separated domains are larger than 15 nm^2.[5c]

Here we report a rapid, accessible method complementary to scanning probe microscopy that uses the electrochemical response of tethered ferrocene redox probes to detect internal hydrogen-bond driven nanoscale phase separation of amide-containing

thiols from alkane thiols over large areas (ca. 1 cm^2). This technique provides a number of key advantages. First, because the electrochemical behavior of the ω-terminal electroactive functional group is strongly dependent on the probe's local environment, this technique allows characterization of interactions on the molecular scale.[23,24] The current-voltage response of the probe can also be used to determine the surface coverage of the adsorbates.[23,24] Second, ferrocene-terminated thiols, such as **1ATC11(O_2C)Fc** (see Chart 1), are synthetically accessible. Third, the gold substrate serves as a convenient electrode. Finally, this non-destructive electrochemical analysis can be performed in situ within minutes on a large section of sample and is not limited to planar substrates.

Chart 1

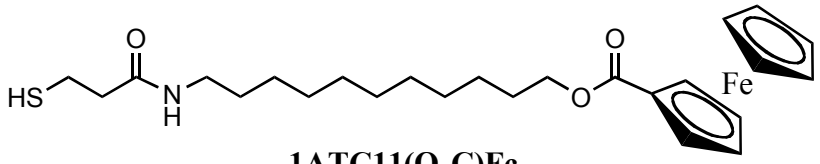

1ATC11(O_2C)Fc

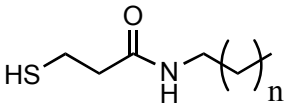

n = 8: **1ATC10**
n = 10 : **1ATC12**

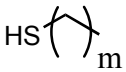

m = 13: **TDT**
m = 15: **HDT**

In this work, we prepared and analyzed several binary SAMs formed from the adsorbates shown in Chart 1. For each SAM, the ferrocene adsorbate, **1ATC11(O_2C)Fc**, was mixed with either an amide-containing thiol (1AT) with a ten or twelve carbon tail (C10 or C12) or an alkanethiol, tetradecanethiol (**TDT**) or hexadecanethiol (**HDT**). We examined SAMs where the ferrocene-terminated probe should either homogeneously mix (e.g. **SAM1-m**, Figure 1) or phase separate (e.g. **SAM2-m**, Figure 1). We explored monolayer

systems where the ferrocene probe was either "matched" (**SAM1-m** and **SAM2-m**, Figure 1) or "exposed" (**SAM1-e** and **SAM2-e**, Figure 1) to further probe how the local environment of the probe influences its electrochemical behavior.

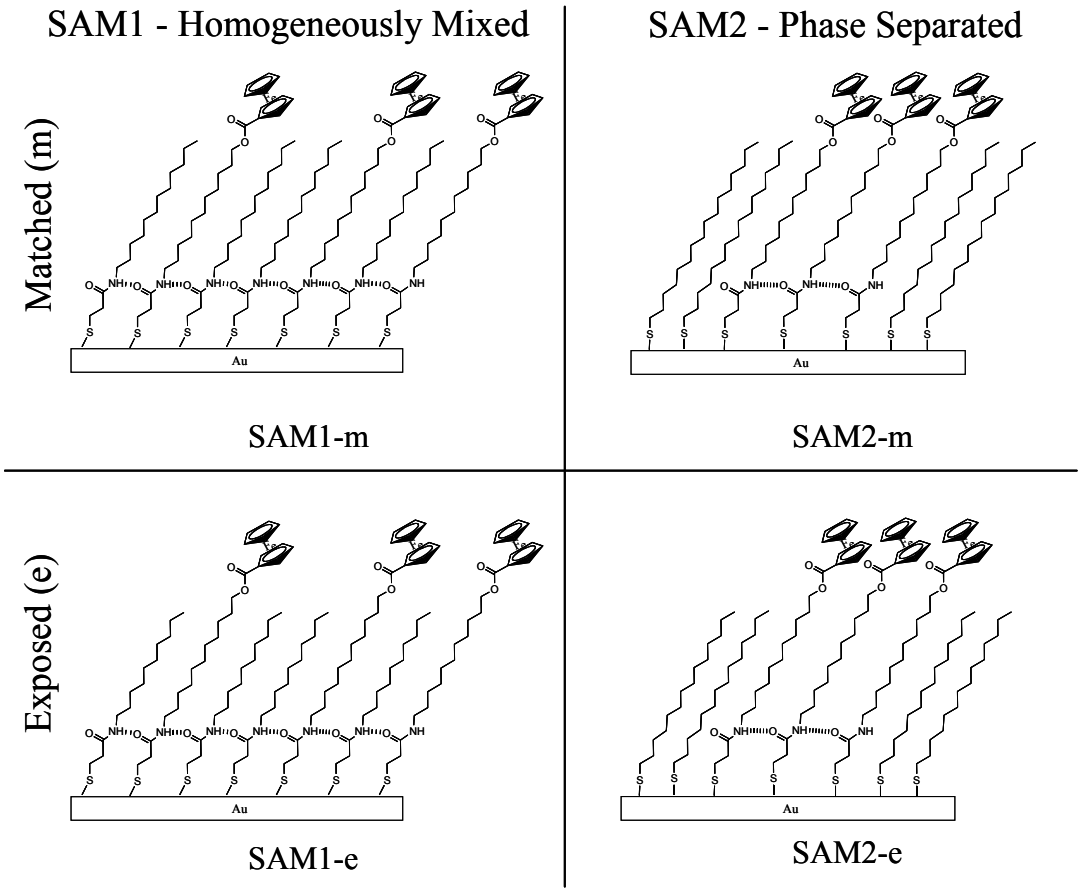

Figure 1. Schematics of **SAM1**, a homogeneously mixed monolayer formed with **1ATC11(O_2C)Fc** and an amide-containing thiol diluent, and **SAM2**, a monolayer where phase separation of ω-terminated groups is driven by buried, interchain hydrogen-bonding formed with **1ATC11(O_2C)Fc** and an alkane thiol diluent. In SAMs with either **1ATC12** (**SAM1-m**) or **HDT** (**SAM2-m**) as the diluent, the length of the adsorbate contains the same number of atoms as the spacer group between the terminal thiol and the ferrocene carboxylate group in **1ATC11(O_2C)Fc**. These are classified as "matched". In SAMs with either **1ATC10** (**SAM1-1e**) or **TDT** (**SAM2-e**) diluent, the electroactive ferrocene group is "exposed" above the top of the diluent adsorbates.

For homogeneously mixed SAMs, the current-voltage behavior was nearly ideal at low ferrocene coverage. In addition, the ferrocene concentration on the surface was directly proportional to the amount of ferrocene-terminated thiol in the soaking solution. In

contrast, for low concentrations of ferrocene, phase-separated monolayers exhibited significantly broader oxidation and reduction peaks, and the ferrocene adsorbate concentration on the surface was significantly less than the concentration in the soaking solution. These results agree with our previous findings from STM studies that showed an underepresentation of the amide component in phase-separated monolayers. Taken together, the data demonstrate that the electrochemical response of tethered redox probes can be used to detect internal hydrogen-bond driven nanoscale phase separation of amide-containing thiols and alkane thiols.

Experimental

Synthesis. Dichloromethane and tetrahydrofuran (THF) were distilled (from calcium hydride and potassium, respectively) before use. All other solvents, starting materials, and reagents were used as received. *S*-triphenylmethylmercapto-3-propionic acid was prepared as described in previous reports.[31]

***N*-dodecyl-3-(*S*-triphenylmethylsulfanyl)propanamide (trityl-1ATC12).** *S*-triphenylmethylmercapto-3-propionic acid (1.08 g, 3.1 mmol), 3-*N'*-dimethylaminopropyl-N-ethylcarbodiimide hydrochloride (EDCI) (0.53 g, 2.8 mmol), and 4-(dimethylamino)-pyridine (DMAP) (0.05 g, 0.41 mmol) were dissolved in 250 mL dichloromethane at room temperature under argon. The reaction solution remained clear and colorless upon the addition of *n*-dodecylamine (0.54 g, 2.9 mmol). After stirring for 16 hours, the reaction solution was washed with 2 x 100 mL 10% HCl, 2 x 100 mL saturated $NaHCO_3$, 100 mL water, and 2 x 100 mL brine. The organic solvent was dried with $MgSO_4$ and then removed to yield a sticky residue. Recrystallization from ethanol/water yielded 1.27 g (88% yield) of white, crystalline product. Melting point 82–

83 °C. ^{1}H NMR (300 MHz, $CDCl_3$). ∂ 7.46-7.42 (m, 6H), 7.33-7.20 (m, 9H), 5.24 (broad, 1H), 3.17 (q, 2H), 2.50 (t, 2H), 2.00 (t, 2H), 1.44 (m, 2H), 1.26 (broad, 18H), 0.89 (t, 3H) ^{13}C NMR (75.5 MHz, $CDCl_3$). ∂ 145.30, 130.22, 128.58, 127.33, 122, 67, 55.61, 40.17, 36.44, 30.18, 29.94, 28.46, 27.53, 23.33.

***N*-decyl-3-(*S*-triphenylmethylsulfanyl)propanamide (trityl-1ATC10).** The procedure for **trityl-1ATC12** was followed except that the reaction was scaled up and *n*-decylamine (3.2 mL, 16.0 mmol) was used. Yield 4.74 g (61% yield) of white, crystalline product. Melting point 81–83 °C. ^{1}H NMR (300 MHz, $CDCl_3$). ∂ 7.46-7.42 (m, 6H), 7.33-7.20 (m, 9H), 5.28 (broad, 1H), 3.17 (q, 2H), 2.51 (t, 2H), 2.02 (t, 2H), 1.45 (m, 2H), 1.27 (broad, 14H), 0.90 (t, 3H) ^{13}C NMR (75.5 MHz, $CDCl_3$). ∂ 170.7, 144.6, 129.6, 127.9, 126.7, 66.8, 39.5, 35.8, 31.8, 29.5, 29.3, 27.8, 26.9, 22.7, 14.1.

1ATC12. Trityl-1ATC12 (0.78 g, 1.51 mmol) was placed in a 100 mL round bottom flask. Trifluoroacetic acid (8 mL) was added, which dissolved the solid and turned the solution bright yellow. When triethylsilane (0.6 mL) was added, the solution became clear and a white precipitate formed. The solvent was removed *in vacuo* and the resulting solid was purified by silica rotary chromatrography using a mixture of hexanes:ethyl acetate to elute, yielding a pure, white solid (0.3178 g, 77% yield). Melting point 61–63 °C. ^{1}H NMR (300 MHz, $CDCl_3$). ∂ 5.58 (broad, 1H), 3.28 (q, 2H), 2.82 (q, 2H), 2.48 (t, 2H), 1.62 (t, 1H), 1.49 (m, 2H), 1.26 (broad, 18H), 0.89 (t, 3H). ^{13}C NMR (75.5 MHz, $CDCl_3$). ∂ 40.5, 39.6, 31.9, 29.6, 29.5, 29.5, 29.3, 29.2, 26.9, 22.6, 20.5, 14.1.

1ATC10. The procedure for **1ATC12** was followed, with 0.500 g of **trityl-1ATC10**. Yield 0.1983 g (78.5% yield) of white, crystalline product. Melting point 43–45 °C. ^{1}H NMR (300 MHz, $CDCl_3$). ∂ 5.58 (broad, 1H), 3.27 (q, 2H), 2.82 (q, 2H), 2.50 (t, 2H),

1.62 (t, 1H), 1.51 (m, 2H), 1.26 (broad, 14H), 0.88 (t, 3H) ^{13}C NMR (75.5 MHz, $CDCl_3$). ∂ 40.5, 39.6, 31.8, 29.6, 29.5, 29.3, 26.9, 22.6, 20.5, 14.1.

11-azoundecan-1-ol. Sodium azide (15.6 g, 240 mmol) and 11-bromoundecan-1-ol (15.1 g, 60 mmol) were refluxed in acetonitrile (250 mL) under nitrogen for 16 hours. After cooling to room temperature, the solvent was removed and the brown residue was extracted with dichloromethane. Evaporation of the dichloromethane yielded a thin, brown oil (12.67 g, 99% yield), which was used in subsequent steps without further purification. ^{1}H NMR (300 MHz, $CDCl_3$). ∂ 3.66 (t, 2H), 3.28 (t, 2H), 1.59 (m, 4H), 1.31 (broad, 14H). ^{13}C NMR (75.5 MHz, $CDCl_3$). ∂ 63.0, 51.4, 32.7, 29.5, 29.4, 29.3, 29.1, 28.8, 26.7, 25.7.

11-aminoundecan-1-ol, 1. Lithium aluminum hydride (2.50 g, 66 mmol) was slowly added to 250 mL THF at room temperature. The reaction was then cooled to 0 °C, purged with argon, and 11-azoundecan-1-ol (8.34 g, 44 mmol) in THF (100 mL) was added dropwise. Workup involved adding sequentially 2.5 mL water, 2.5 mL 15% NaOH, and 7.5 mL water. (The mixture was thoroughly stirred between each addition.) The suspension was filtered and the solvent removed from the filtrate to yield a white solid. The crude product was recrystallized from THF/heptane to yield the purified compound (5.96 g, 81% yield). Melting point 80–82 °C. ^{1}H NMR (300 MHz, $CDCl_3$). ∂ 3.66 (t, 2H), 2.69 (t, 2H), 1.57 (m, 2H) 1.44 (m, 2H), 1.29 (broad, 14H). ^{13}C NMR (75.5 MHz, $CDCl_3$). ∂ 63.5, 42.4, 34.0, 33.0, 29.8, 29.7, 29.7, 29.6, 27.1, 26.0.

***N*-(undecyl-11-ol)-3-(*S*-triphenylmethylsulfanyl)propanamide, 2.** EDCI (8.47 g, 44 mmol), DMAP (0.49 g, 4.0 mmol), and **1** (7.74 g, 41 mmol) were dissolved in 200 mL dichloromethane at room temperature. A mixture of S-triphenylmethylmercapto-3-

propionic acid (15.23 g, 44 mmol) in 200 mL dichloromethane was added dropwise. After stirring for 16 hours, the reaction solution was washed sequentially with 2 x 100 mL 10% HCl, 2 x 100 mL saturated $NaHCO_3$, 100 mL water, and 2 x 100 mL brine. The organic solvent was dried with $MgSO_4$ and a small amount of basic Al_2O_3 and then removed to yield a sticky off-white product (18.12 g, 85%). Melting point 66–68 ^oC ^1H NMR (300 MHz, $CDCl_3$). ∂ 7.46-7.42 (m, 6H), 7.33-7.20 (m, 9H), 5.27 (broad, 1H), 3.65 (t, 2H), 3.16 (q, 2H), 2.50 (t, 2H), 2.01 (t, 2H), 1.56 (m, 2H), 1.44 (m, 2H), 1.26 (broad, 14H). ^{13}C NMR (75.5 MHz, $CDCl_3$). ∂ 170.8, 144.6, 129.6, 127.9, 126.6, 66.8, 39.5, 35.7, 32.7, 29.5, 29.4, 29.3, 27.8, 26.8, 25.7.

11-{*N*-[3-(*S*-triphenylmethylsulfanyl)]propionylamino} undecyl ferrocene carboxylate (trityl-1ATC11(O_2C)Fc). Ferrocenecarboxylic acid (2.754 g, 12 mmol) was placed in a 500 mL flask. Oxalyl chloride (15 mL, 172 mmol) was added and the mixture was stirred for 1 hour. The excess oxalyl chloride was removed *in vacuo*, and the red residue was dissolved in 100 mL dichloromethane. Triethylamine (1 mL, 7 mmol) and DMAP (0.0673 g, 0.5 mmol) were added and the solution was stirred under argon for ~20 minutes. A solution of **2** (2.83 g, 5.47 mmol) in 200 mL dichloromethane was added dropwise. After stirring for 48 hours, the reaction solution was filtered through basic Al_2O_3 and celite. The desired product was concentrated and dried *in vacuo* for 24-72 hours to yield a sticky, red gum (2.73 g, 68% yield). ^1H NMR (300 MHz, $CDCl_3$). ∂ 7.46-7.42 (m, 6H), 7.33-7.20 (m, 9H), 5.24 (broad, 1H), 4.81 (t, 2H), 4.38 (t, 2H), 4.21 (t, 2H), 4.20 (s, 5H), 3.16 (q, 2H), 2.50 (t, 2H), 2.00 (t, 2H), 1.72 (m, 2H), 1.44 (m, 2H), 1.26 (broad, 12H). ^{13}C NMR (75.5 MHz, $CDCl_3$). ∂ 171.7, 170.7, 144.6, 129.5,

127.8, 126.6, 71.4, 71.1, 70.0, 69.6, 66.7, 64.2, 39.4, 35.7, 29.5, 29.4, 29.2, 28.9, 27.7, 26.8, 25.8.

1ATC11(O_2C)Fc. Deprotection of **trityl-1ATC11(O_2C)Fc** (0.38 g, 0.53 mmol) was performed using same procedure as described for 1ATC12 and 1ATC10, with care taken to exclude oxygen during both deprotection and purification, to yield a viscous orange oil (0.15 g, 60% yield). ^{1}H NMR (300 MHz, $CDCl_3$) ∂ 5.62 (broad, 1H), 4.81 (t, 2H), 4.40 (t, 2H) 4.21 (t, 2H), 4.20 (s, 5H), 3.27 (q, 2H), 2.83 (q, 2H), 2.49 (t, 2H), 1.73 (m, 2H) 1.62 (t, 1H), 1.51 (m, 2H), 1.30 (broad, 12H). ^{13}C NMR (75.5 MHz, $CDCl_3$) 71.4, 71.1, 69.9, 64.2, 39.5, 29.5, 29.4, 29.3, 29.1, 28.7, 26.8, 25.9, 20.5.

Monolayer Preparation. Freshly cleaved mica substrates with a freshly deposited (150 nm) gold film were used for monolayer formation. Immediately prior to use, gold substrates were UV/ozone cleaned for 10 minutes, rinsed with ethanol and dried with argon. The substrates were then soaked in an ethanol solution containing 1 mM total thiol [1ATC11(O_2C)Fc and a non-electroactive diluent], where the mole fraction of the ferrocene-terminated thiol to the total thiol concentration (χ_{Fc}) varied from 0 to 1. The monolayer samples were removed from the thiol solutions after soaking for a minimum of 2 days, rinsed with ethanol, and then dried under argon. No differences were observed between samples that soaked for 2 days and those that soaked for several weeks.

Electrochemical Measurements. Cyclic voltammograms were recorded with a BAS 100B electrochemical workstation. Monolayer samples were clamped to an O-ring joint on the electrochemical cell. A fresh Viton O-ring was used for each sample and the ring defined the working electrode area (0.78 cm^2). The Au surface served as the working

electrode. The supporting electrolyte (1M $HClO_4$), a calomel reference electrode (with 3M NaCl), and a Pt auxiliary electrode were placed in the electrochemical cell.

The amount of the electroactive species in the SAM was quantified from the cyclic voltammograms.[24] After subtracting a background scan (of an all diluent molecule monolayer) to correct for the charging current, the area under the oxidation peak was integrated. The area was then divided by the scan rate to obtain the amount of charge (in $\mu C/cm^2$) passed through the SAM for the ferrocene/ferrocinium couple. The ferrocene coverage in the SAM was calculated by dividing the surface charge density by the electron charge. All electrochemical data presented are the averages of at least three measurements and have the charging current subtracted. The voltammograms are plotted using the American convention, with the cathodic current positive and the more positive potentials to the left.

Results and Discussion

Our primary goal for these experiments was to develop a method to detect phase separation of ω-terminal functional groups in self-assembled monolayers on gold surfaces. By developing a quick, easily accessible method complementary to scanning probe microscopy, we are able to detect thiol adsorbate phase separation in SAM systems.

Experimental Design

Thiol adsorbates with a pendant ferrocene group have been used to probe the composition,[23] structure,[9,24,25] and properties[26,27] of mixed thiol monolayers on gold substrates. Previous work by Chidsey and coworkers demonstrated that when ferrocene groups are well-separated and do not interact with one another, a narrow, symmetric

oxidation peak with an ideal full-width at half height (FWHH) of 90 mV is obtained.[24,32,33] As the concentration of the ferrocene adsorbate on the surface increases, the resulting voltammograms become asymmetric, the peaks broaden and the peak separation increases. These observed phenomena are likely due to double layer effects. [34] Using models first developed by Smith and White,[35] Finklea performed linear sweep voltammetry (LSV) simulations to demonstrate that the changes observed by Chidsey are due to a rapid increase in the surface charge during oxidation.[34] The surface charge effectively decreases the potential difference between the remaining unoxidized ferrocenes and the surface, thus a higher applied bias is required for oxidation of these ferrocenes. As the fraction of ferrocene on the surface was increased from 10% to 100%, these double layer effects were shown to shift the oxidation peak to more positive potentials and increase the FWHH of the ferrocene oxidation peak by 275 mV.

Based on Chidsey's observation that monolayers with high ferrocene concentration demonstrate broadened oxidation peaks and Finklea's explanation of the double layer effects responsible for this phenomenon, we predicted that ferrocene redox probes could be used to probe phase separation. Because phase separated monolayers have areas of high ferrocene concentration, local double layer effects should occur within these domains during oxidation. At low ferrocene surface coverages, phase separated monolayers should demonstrate broadened oxidation and reduction peaks when compared to the voltametric response of homogeneously mixed monolayers. Double layer effects should also cause a small shift of the formal potential (average of the anodic and cathodic peak potentials) to more positive potentials.[34] Previous STM studies of methyl terminated, amide-containing phase separated monolayers,[12] indicate that we

should see an underrepresentation of the ferrocene component of the surface when it is the minority component in the soaking solution.

To probe how nanoscale phase separation influences the electrochemical response of the tethered redox probe, four monolayer systems were investigated. In each system the amide-containing, ferrocene-terminated thiol adsorbate, 11-[*N*-(3-*S*-tritylsulfanyl)propionylamino]undecyl ferrocene carboxylate (**1ATC11(O_2C)Fc**, see Chart 1), was mixed with either an amide containing alkanethiol (**1ATC12** or **1ATC10**, see Chart 1) or an alkanethiol (**HDT** or **TDT**), where the mole fraction (χ_{Fc}) of the electroactive ferrocene-terminated thiol was varied from 0 to 1. When both the ferrocene component and the diluent molecule contained an amide group, the adsorbates were expected to mix homogeneously (**SAM1**, Figure 1). When the diluent molecule was an alkanethiol, the adsorbates should phase separate (**SAM2**, Figure 1), based on prior STM work.[12] Because the local environment of redox probes has been shown to influence their electrochemical response,[24,32,33] we examined systems where the alkyl chain length of the diluent was the same as for the redox probe ("matched", **SAM1-m** and **SAM2-m**) and where the diluent chain length was shorter than the alkyl chain of the redox probe ("exposed", **SAM1-e** and **SAM2-e**, Figure 1). When comparing **SAM1** (homogeneously mixed) to **SAM2** (phase separated) we found similar results for both the matched and exposed monolayers, so, for the sake of simplicity, we have chosen to focus on the matched SAMs in this report. The results for the exposed system are provided in the Supporting Information.

To determine the behavior of the ferrocene redox probe in an ideal, homogeneously mixed monolayer, we examined monolayers of **SAM1-m** (**1ATC11(O_2C)Fc** and

1ATC12) on freshly prepared gold substrates. Figure 2a shows a representative set of cyclic voltammograms for the electrochemical response as χ_{Fc} was varied from 0 to 1.[36] The voltammograms in Figure 2a were obtained with a 10 mV/s scan rate. Neither the general features nor the shape of the cyclic voltammograms changed with scan rates up to 100 mV/s. The monolayers were also stable under the characterization conditions, as only small (<5%) changes were observed with repeated scanning. At a 10 mV/s scan rate, very little peak separation (<5 mV) was observed between the ferrocene oxidation and ferricenium reduction in all monolayers. The lack of peak separation indicates that the rate of electron transfer between the terminal ferrocene and the gold substrate is fast on the experiment time scale.[24]

As shown in Figure 2, increasing the χ_{Fc} in the soaking solutions for monolayers prepared with **1ATC11(O_2C)Fc** and the **1ATC12** diluent (**SAM1-m**) lead to several changes in the electrochemical response. As χ_{Fc} was increased in the soaking solutions, the ferrocene oxidation peak current increased and the peak shifted to more positive potentials. Both the oxidation and reduction peaks also significantly broaden as the amount of the ferrocene-terminated thiol increases in the soaking solution. At low χ_{Fc} (<0.25 mole fraction of **1ATC11(O_2)Fc**) the peaks are smooth, symmetrical, and have a full width at half height (FWHH) less than 110 mV. At high χ_{Fc}, the peaks are not smooth and, in some cases, appear as two nearly distinguished, overlapping peaks (Figure 2a, $\chi_{Fc} > 0.75$). This peak splitting has been reported elsewhere in the literature, and is generally attributed to inhomogeneity in ferrocene solvation.[34] The FWHH also increases to 250 mV as χ_{Fc} approaches unity. The nearly ideal peak separation (ΔE_p), shape, and FWHH at low ferrocene coverages indicate that the redox centers are homogeneously

distributed throughout the monolayer and are completely consistent with Chidsey's studies of dilute ferrocene monolayers.[24,32,33]

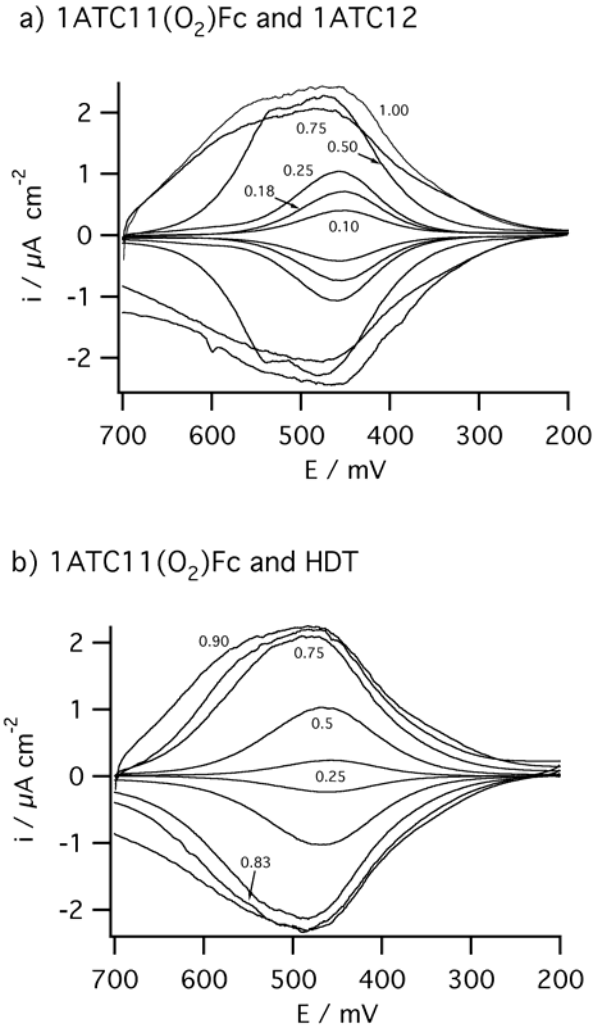

Figure 2. Cyclic voltammograms of self-assembled monolayers of a) **1ATC11(O_2C)Fc** and **1ATC12** (**SAM1-m**); and, b) **1ATC11(O_2C)Fc** and **HDT** (**SAM2-m**). In both cases, the SAMs were formed from ethanol solutions containing various mole fractions of the ferrocene-terminated thiol, **1ATC11(O_2C)Fc**(χ_{Fc}). Each voltammogram has been normalized for the working electrode surface area after subtracting the charging current. Supporting electrolyte: 1 M $HClO_4$; Reference electrode: calomel with 3 M NaCl; Auxiliary: Pt; Scan rate = 10 mV/s.

As we initially expected, the ferrocene electrochemical response in **SAM1** reflects a homogeneous distribution of the ω-terminated thiol throughout the monolayer. As the ferrocene coverage closely approximates the χ_{Fc} in the soaking solution, at the lowest

level of ferrocene (χ_{Fc} = 0.1) the electroactive groups are essentially isolated within the monolayer. Increases in χ_{Fc} in the soaking solutions lead to a steady increase in the amount of ω-terminated ferrocene adsorbate in the monolayer and a concomitant increase in the FWHH of the oxidation peak, which is typically observed for homogeneously mixed monolayers.[24] In investigating **1ATC11(O_2C)Fc** in homogeneously mixed monolayers**,** we found that the diluent chain length has no influence on ferrocene surface coverage (see Supporting Information).

Influence of phase separation on ferrocene surface coverage

Figure 2b shows the voltammetric response of mixed monolayers prepared with **1ATC11(O_2C)Fc** and the alkanethiol, **HDT** (**SAM2-m**). At low values of χ_{Fc}, the maximum oxidation current for SAMs prepared from soaking solutions with the same χ_{Fc} are different for the two systems. Figure 3 shows that at χ_{Fc} = 0.25, the magnitude of the oxidation peak for **SAM1-m** is much greater than that for **SAM2-m**, which indicates that there is significantly more ferrocene on the surface when the diluent and probe molecules both contain an amide.

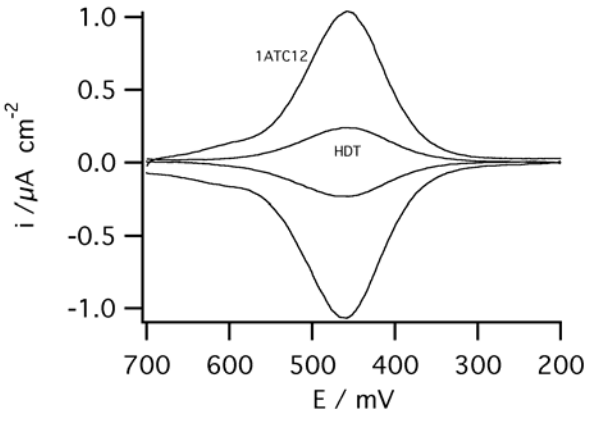

Figure 3. Cyclic voltammograms of self-assembled monolayers of **1ATC11(O_2C)Fc** and either **1ATC12** or **HDT**. In both cases, the SAMs were formed from a soaking solution containing 0.25 mole fraction of the ferrocene-terminated thiol. Each

voltammogram has been normalized for the working electrode surface area after subtracting the charging current. Supporting electrolyte = 1 M $HClO_4$; Reference electrode = calomel with 3 M NaCl; Auxiliary = Pt; Scan rate = 10 mV/s.

In Figure 4, the ferrocene coverage is plotted as a function of χ_{Fc} in the soaking solution for both systems: the all-amide monolayers with **1ATC12** (**SAM1-m**) and mixed SAMs with **HDT** (**SAM2-m**). Several observations can be made from Figure 4. First, the amount of ferrocene in both **SAM1-m** and **SAM2-m** monotonically increases with increasing χ_{Fc} in the soaking solution. Second, for $\chi_{Fc} < 0.25$, the ferrocene coverage for the all-amide system increases as χ_{Fc} in the soaking solution increases. The amount of ferrocene in SAMs that contain the alkane thiol **HDT** diluent is significantly less than the ferrocene present in monolayers prepared with **1ATC12** for the same concentration of ferrocene in the soaking solution, This difference indicates that the amide-containing, ferrocene-terminated thiols are underrepresented in the phase separated monolayer relative to the soaking solution concentration. As the amount of ferrocene in the soaking solution approaches $\chi_{Fc} = 1$, the ferrocene coverages for the two types of SAMs (SAM1-m and SAM2-m) are nearly identical. We observed this same underrepresentation at low amide concentrations in previous STM studies of phase separated monolayers of 1ATC9 and decanethiol.[12]

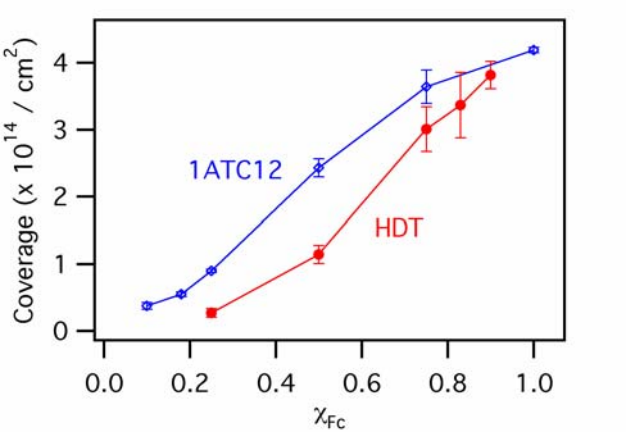

Figure 4. Plot of ferrocene charge density and surface coverage as a function of χ_{Fc} in the ethanol soaking solution for mixed, matched monolayers containing **1ATC11(O$_2$C)Fc** and either **1ATC12 [SAM1-m** (◇)] or **HDT [SAM2-m** (●)]. The error bars represent the standard deviation of the ferrocene coverage for the trials.

Influence of phase separation on ferrocene electrochemical behavior

To probe the local environment of the ferrocene redox probe, the FWHH of the oxidation peak was determined from the cyclic voltammograms. In Figure 5, the FWHH values are plotted against the average ferrocene surface coverage (as obtained from Figure 4) for both **SAM1-m** and **SAM2-m**. For monolayers prepared with the ferrocene-probe thiol and **1ATC12** (**SAM1-m**), the FWHH values at low ferrocene coverages are close to the 90 mV theoretical value for a reversible one-electron electrochemical process,[24,32,33] while the FWHH for SAM2-m are significantly larger. At low ferrocene coverages, the difference in FWHH values between the two systems is ca. 30 mV, while at high coverages there is no detectable difference.

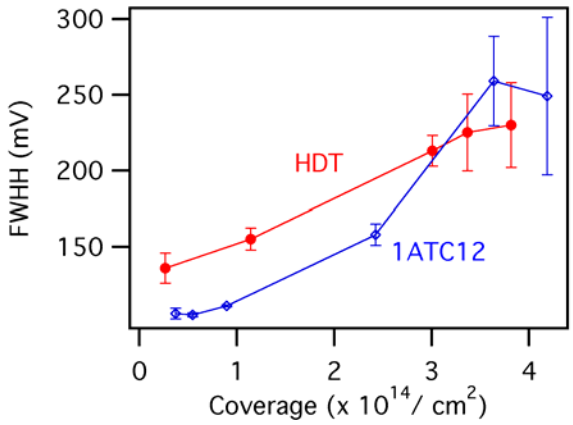

Figure 5. Plot of full width at half height (FWHH) for the ferrocene oxidation peak as a function of ferrocene coverage for mixed, matched monlayers containing **1ATC11(O_2C)Fc** and either **1ATC12 [SAM1-m** (◇)] or **HDT [SAM2-m** (●)**].** The error bars represent the standard deviation of the FWHH for the trials.

Broader peaks reflect a multiplicity of ferrocene electrochemical environments resulting from the influence of neighboring electroactive groups. As we initially expected, the double layer effects also cause a small shift in the formal potential of the ferrocene (see Figure 6). Based on these observations, the broader, shifted peaks for **SAM2** indicate that even at low ferrocene coverages, the ferrocene electrochemistry is significantly influenced by other electroactive thiols, which indicates the presence of ferrocene-rich, phase separated domains.

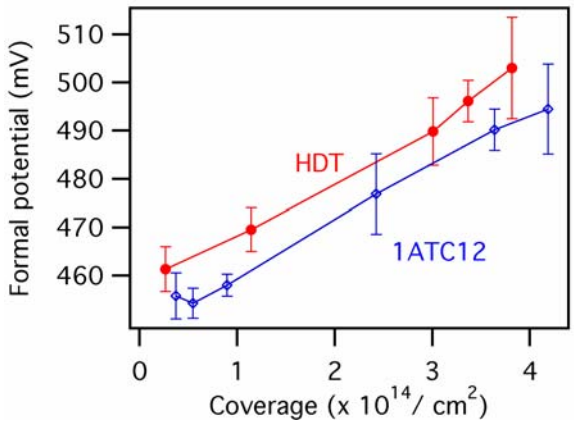

Figure 6. Plot of the formal potential (average of the anodic and cathodic peak potentials) for the ferrocene probe vs. ferrocene coverage for mixed, matched monlayers

containing **1ATC11(O_2C)Fc** and either **1ATC12 [SAM1-m** (◇)] or **HDT [SAM2-m (●)].** The error bars represent the standard deviation of the formal potentials for the trials.

The significant difference in the FWHHs observed for homogeneously mixed and phase separated monolayers demonstrates that the voltammetric response of tethered ferrocene redox probes can be used to determine whether phase separation is occurring between components in a monolayer.

Influence of Matched versus Exposed Ferrocene Redox Probes

For the series of "exposed" monolayers, **SAM1-e** and **SAM2-**e (SAMs with **1ATC11(O_2C)Fc** and either **1ATC10** or **TDT**, respectively), the electrochemical data is qualitatively similar to the results obtained for the "matched" systems. At low values of χ_{Fc} ($\leq$0.5) in the soaking solution, ferrocene coverage is lower for SAMs with an alkane thiol diluent than for monolayers prepared with **1ATC10**. The FWHH is also ca. 30 mV higher for **SAM2-e** structures than for those with **TDT** diluent. When the matched and exposed monolayers are compared, however, the FWHH for matched monolayers is 20 – 80 mV greater than the values for the exposed systems for both **SAM1** and **SAM2**. The origin of this difference in the FWHH can be explained in a number of ways, including differences in electron transfer rates,[37] steric interactions, or differences in solvation (see Supporting Information for a more complete discussion of potential causes). What is clear from the comparison of the matched and exposed monolayers is that while both exposed and matched diluents can be used to probe for phase separation, diluents with identical lengths must be used for both the control experiment (homogeneously mixed SAM) and the SAM under investigation to conclusively determine whether or not phase separation is occurring in new systems. Regardless of the diluent chain length selected (matched or exposed), however, at low ferrocene surface coverages, phase separated

monolayers demonstrate statistically larger FWHHs when compared to homogeneously mixed monolayers.

Summary

In summary, we have developed a powerful, yet flexible method that can be used to study electroactive, nanoscale features in thiol/Au SAMs. We have demonstrated that cyclic voltammetry can be used to detect surface concentration and phase separation in mixed, binary monolayers. We have also shown that the relative length of the diluent thiol affects the electrochemical behavior of the redox probe. We are currently using cyclic voltammetry to detect phase separation of electrochemically active ω-terminal functional groups in related amide-containing SAMs.

Acknowledgement. We thank the NSF IGERT fellowship (CEI), the Department of Education GAANN fellowship (CEI) and the George Fox University Faculty Development Fund. We also thank Robert Clegg for helpful discussions and Whittney Harris for assistance with some measurements.

Supporting Information Available: Electrochemical data for **SAM1-e** and **SAM2-e** (Figure S1) as well as a comparison of ferrocene surface coverage to soaking solution concentration (Figure S2) and a comparison of FWHH as well as formal potential to ferrocene surface coverage (Figures S3 and S4) for the exposed homogeneously mixed and phase separated monolayers. The Supporting Information also contains a discussion of the factors that may influence the differences observed in FWHH for the matched versus exposed monolayers (Figure S5) as well as a plot of ferrocene surface coverage versus soaking solution concentration for all four monolayer systems. This material is available free of charge via the Internet at http://pubs.acs.org.

Table of Contents Figure

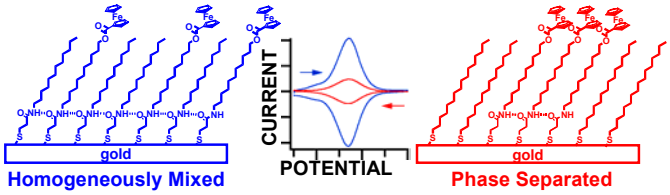

References

1. Ulman, A. *Introduction to Ultrathin Organic Films: From Langmuir-Blodgett to Self-Assembly*; Academic: New York, 1991.

2. a) Xia, Y.; Whitesides, G.M. *Angew. Chem., Int. Ed. Engl.* **1998**, *37*, 550; b) Zhao, X.M.; Xia, Y.; Whitesides, G.M. *J. Mater. Chem.* **1997**, *7*, 1069; c) Kumar, A.; Biebuyck, H.A.; Whitesides, G.M. *Langmuir* **1994**, *10*, 1498.

3. Tan, J.L.; Tien, J.; Chen, C.S. *Langmuir* **2002**, *18*, 519.

4. a) Yang, D-F; Morin, M. *J. Electroanal. Chem.* **1998**, *441*, 173; b) Zhong, C-J; Zak, J.; Porter, M.D. *J. Electroanal. Chem.* **1997**, *421*, 9; c) Yang, D-F; Morin, M. *J. Electroanal. Chem.* **1997**, *429*, 1; d) Walczak, M.W.; Alves, C.A.; Lamp, B.D. Porter, M.D. *J. Electroanal. Chem.* **1995**, *396*, 103; e) Widrig, C.A.; Chung, C.; Porter, M.D. *J. Electroanal. Chem.* **1991**, *310*, 335.

5. a) Imabayashi, S.; Hobara, D.; Kakiuchi, T. *Langmuir* **2001**, *17*, 2560; b) Hobara, D.; Sasaki, T.; Imabayashi, S. *Langmuir* **1999**, *15*, 5073; c) Hobara, D.; Ota, M. Imabayashi, S.; Niki, K.; Kakiuichi, T. *J. Electroanal. Chem.* **1998***, 444*, 113.

6. Zhang,Y; Salaita, K.; Lim, J-H; Mirkin, C.A. *Nano Letters* **2002**, *2*, 1389.

7. a) Smith, J.C.; Lee, K-B; Wang, O.; Finn, M.G.; Johnson, J.E.; Mrksich, M.; Mirkin, C.A. *Nano Letters* **2003**, *3*, 883; b) Hong, S.; Mirkin, C.A. *Science* **2000**, *288*, 1808; c) Piner, R.; Zhu, J.; Xu, F.; Hong, S.; Mirkin, C.A. *Science* **1999**, *283*, 661.

8. Gorman, C.B.; Carroll, R.L.; Fuierer, R. *Langmuir* **2001**, *17*, 6923.

9. Bar, G.; Rubin, S.; Taylor, T.N.; Swanson, B.I.; Zawodzinski, T.A.; Chow, J.T.; Ferraris, J.P. *J. Vac. Sci. Technol. A* **1996**, *14*, 1794.

10. Schoer, J.K.; Zamborini, F.P.; Crooks, R.M. *J. Phys. Chem.* **1996**, *100*, 11086.

11. Reed, S.M.; Clegg, R.S.; Hutchison, J.E. in *Molecules as Components of Electronic Devices*; Lieberman, M., Ed.; American Chemical Society: Washington DC, 2002, 36.

12. a) Lewis, P.A.; Smith, R.K.; Kelly, K.F.; Bumm, L.A.; Reed, S.A.; Clegg, R.S.; Gunderson, J.D.; Hutchison, J.E.; Weiss, P.S. *J. Phys. Chem. B* **2001**, *105*, 10630; b) Smith, R.K.; Reed, S.A.; Lewis, P.A.; Monnell, J.D.; Clegg, R.S.; Kelly, K.F.; Bumm, L.A.; Hutchison, J.E.; Weiss, P.S. *J. Phys. Chem. B* **2001**, *105*, 1119.

13. a) Mrksich, M. *Curr. Op. Chem. Biol.* **2002**, *6*, 794; b) Houseman, B. T.; Mrksich, M. *Biomaterials*, **2001**, *22*, 943; c) Koo, L.Y.; Irvine, D. J.; Mayes, A. M.; Lauffenburger, D. A.; Griffith, L. G. *J. Cell. Sci.* **2002**, *115*, 1423.

14. Clegg, R.S.; Hutchison, J.E. *J. Am. Chem. Soc.* **1999**, *121*, 5319.

15. a) Strannick, S.J.; Parikh, A.N.; Tao, Y-T; Allara, D.L.; Weiss, P.S. *J. Phys. Chem.* **1994**, *98*, 7636; b) Strannick, S.J.; Kamna, M.M.; Krom, K.R.; Parikh, A.N.; Allara, D.L.; Weiss, P.S. *J. Vac. Sci. Technol. B* **1994**, *12*, 2004.

16. Chi, L.F.; Anders, M.; Fuchs, H.; Johnston, R.R.; Ringsdorf, H. *Science* **1993**, *259*, 213.

17. Fleming, M.S.; Walt, D.R. *Langmuir* **2001**, *17*, 4836.

18. Knobler, C.M. *Science* **1990**, *249*, 870.

19. Merkel, R.; Sackmann, E. *J. Phys. Chem.* **1994**, *98*, 4428.

20. a) Tanhauanpää, K.; Cheng, K.H.; Anttonen, K.; Virtanen, J.A.; Somerharju, P. *Biophysical J.* **2001**, *81*, 1501; b) Samsanov, A.V.; Mihaloyov, I.; Cohen, F.S. *Biophysical J.* **2001**, *81*, 1486.

21. a) Wellsted, H.; Sitsen, E.; Caragheorgheopol, A.; Chechik, V. *Anal. Chem.* **2004**, *76*, 2010; b) Chachaty, C.; Wolf, C. *Trends Phys. Chem.* **2001**, *8*, 107.

22. Chechik, V.; Wellsted, H.J.; Korte, A.; Gilbert, B.G.; Caldararu, H.; Ionita, P.; Caragheorgheopol, A. *Farad. Discuss.* **2003**, *125*, 279; b) Veksli, Z.; Andreis, M. *Prog. Polym. Sci.* **2000**, *25*, 949.

23. Collman, J.P.; Devaraj, N.K.; Chidsey, C.E.D. *Langmuir* **2004**, *20*, 1051.

24. Chidsey, C.E.D.; Bertozzi, C.R.; Putvinski, T.M.; Mujsce, A.M. *J. Am. Chem. Soc.* **1990**, *112*, 4301.

25. a) Auletta, T.; van Veggel, F.C.J.M.; Reinhoudt, D.N. *Langmuir* **2002**, *18*, 1288; b) Ye, S.; Haba, T.; Sato, Y.; Shimazu, K.; Uosaki, K. *Phys. Chem. Chem. Phys.* **1999**, *1*, 3653.

26. a) Smalley, J.F.; Finklea, H.O.; Chidsey, C.E.D.; Linford, M.R.; Creager, S.E.; Ferraris, J.P.; Chalfant, K.; Zawodzinsk, T.; Feldberg, S.W.; Newton, M.D. *J. Am. Chem. Soc.* **2003,** *125*, 2004; b) Sek, S.; Palys, B.; Bilewicz, R. *J. Phys. Chem. B* **2002**, *106*, 5907; c) Sek, S.; Misicka, A.; Bilewicz, R. *J. Phys. Chem. B* **2000**, *104*, 5399; d) Napper,

A.M.; Liu, H.; Waldeck, D.H. *J. Phys. Chem. B* **2001**, *105*, 7699; e) Kondo, T.; Kanai, T.; Uosaki, K. *Langmuir* **2001**, *17*, 6317.

27. a) Oh, S-K.; Baker, L.A.; Crooks, R.M. *Langmuir*, **2002**, *18*, 6981; b) Berchmans, S.; Ramalechume, C; Lakshmi, V.; Yegnaraman, V. *J. Mater. Chem.* **2002**, *12*, 2538; c) Beer, P.D.; Davis, J.J.; Drillsma-Milgrom, D.A.; Szemes, F. *Chem. Commun. 16,* **2002**, 1716; d) Li, Q.; Mathur, G.; Homsi, M.; Surthi, S.; Misra, V.; Malinovskii, V.; Schweikart, K.H.; Yu, L.; Lindsey, J.S.; Liu, Z.; Dabke, R.B.; Yasseri, A.; Bocian, D.F.; Kuhr, W.G. *Appl. Phys. Lett.* **2002**, *81*, 1494.

28. Kittredge, K.W.; Fox, M.A.; Whitesell, J.K. *J. Phys. Chem. B* **2001**, *105*, 10594.

29. Imahori, H.; Nishimura, Y.; Norieda, H.; Karita, H.; Yamazaki, I.; Sakata, Y.; Fukuzumi, S. *Chem. Comm.* **2000**, *8,* 661.

30. Zhang, J.; Whitesell, J.K.; Fox, M.A. *Chem. Mater.* **2001**, *13*, 2323.

31. Reed, S.M. Ph.D. Dissertation **2001**, University of Oregon, Department of Chemistry, 65.

32. Chidsey, C.E.D.; Science **1991**, 251, 919.

33. Murray, R.W. in *Electroanalytical Chemistry, Vol. 13*; Bard, A.J., Ed.; Marcel Dekker: New York, 1984, 191.

34. Finklea, H.O. in *Electroanalytical Chemistry, Vol. 19*; Bard, A.J., Ed.; Marcel Dekker: New York, 1996, 109.

35. Smith, C.P.; White, H.S. *Anal. Chem.* **1992**, *64*, 2398.

36. The voltammograms in Figures 2 and 3 were obtained by subtracting a background scan to remove the charging current, then dividing by the scan rate.

37. Finklea, H.O.; Liu, L.; Ravenscroft, M.S.; Punturi, S. *J. Phys. Chem.* **1996**, *100*, 18852.